

Vacuum Rabi splitting in a plasmonic cavity at the single quantum emitter limit

Kotni Santhosh^{1,*}, Ora Bitton^{2,*}, Lev Chuntonov^{3,*} and Gilad Haran¹

¹Departments of Chemical Physics and ²Chemical Research Support, Weizmann Institute of Science, Rehovot, Israel, and ³Schulich Faculty of Chemistry, Technion-Israel Institute of Technology, Haifa, Israel.

Correspondence and requests for materials should be addressed to G.H.

(gilad.haran@weizmann.ac.il).

*These authors contributed equally to this work.

The strong interaction of individual quantum emitters with resonant cavities is of fundamental interest for understanding light matter interactions¹, as well as for quantum information processing^{2,3} and quantum communication applications^{4,5}. Plasmonic cavities hold the promise of attaining the strong coupling regime even under ambient conditions and within subdiffraction volumes. Recent experiments revealed strong coupling between individual plasmonic structures and multiple organic molecules^{6,7}, but so far strong coupling at the limit of a single quantum emitter has not been reported. Here we demonstrate vacuum Rabi splitting, a manifestation of strong coupling, using silver bowtie plasmonic cavities loaded with semiconductor quantum dots (QDs). A transparency dip is observed in the scattering spectra of individual bowties with one to a few QDs in their gaps. Rabi splitting values as high as 180 meV are registered with a single QD. These observations are verified by polarization-dependent experiments and validated by electromagnetic calculations.

The interaction of a quantum emitter with an optical cavity falls within the realm of cavity quantum electrodynamics¹. The strength of the interaction depends on the ratio of the quality factor of the cavity to the mode volume, Q/V . In optical cavities made of e.g. photonic crystals⁸ or micropillars⁹ the fundamental laws of diffraction set a strict limitation on the cavity size, which cannot be smaller than half the wavelength of the interacting photon. This in turn limits how small V can be, and mandates a very high Q in order to attain the strong coupling regime. Obtaining such a high quality factor requires demanding experimental conditions such as cryogenic temperatures and ultra-narrow frequency light sources. Cavities made of materials that can sustain surface plasmon (SP) excitations can beat the diffraction limit by focusing intense electromagnetic fields into volumes much smaller than the wavelength of light¹⁰. Such cavities should simplify considerably the experimental conditions

required for strong light-matter interactions, and may allow quantum optical experiments to be conducted under ambient conditions.

Noble metals are used for generating structures sustaining SPs at visible wavelengths. While the SP relaxation times in such structures are ultrafast, severely limiting Q, their mode volume is drastically reduced compared to photonic cavities. Many experiments reported strong coupling between plasmonic systems and multiple molecules (reviewed in ref. ¹¹). Recently, strong coupling has also been probed at the level of a single plasmonic device. Thus, Halas and coworkers used gold dimers and molecular J-aggregates to observe a Rabi splitting of ~ 230 meV ⁶. Shegai and coworkers observed strong coupling using either a silver nanorod ¹² or a silver nanoprism ⁷, in both cases employing J-aggregates as the quantum emitters. In all of these experiments the interaction involved *hundreds of quantum emitters* or more. However, for quantum information operations one needs to approach *the limit of a single quantum emitter* coupled to the cavity. This is the aim of the current work.

Inspired by recent computational studies that suggested that strong coupling with individual emitters can be achieved in the gaps of plasmonic structures¹³, we turned to silver bowties, which can be fabricated with a small gap¹⁴. Silver is preferred as a material for plasmonic devices due to its relatively low surface plasmon damping and hence the high achievable quality factors of such devices compared to other metals¹⁵. By varying the structural parameters of the bowties, including side length and gap size, the localized surface plasmon excitations of bowties manufactured by electron-beam lithography can be tuned to resonance with the quantum emitter of choice, while maintaining gaps of the order of ~ 20 nm. To achieve strong coupling the quantum emitter should possess a large oscillator strength and a narrow linewidth. QDs have several advantages over organic emitters in relation to the aforementioned characteristics¹⁶, and are also significantly more photostable. Commercially-available CdSe/ZnS QDs were employed in the present study. Optical spectroscopy and

electron microscopy studies showed that the sample is mildly heterogeneous and the diameter of the QD varies between 6 and 8 nm.

To position QDs within the gaps of bowties we made use of interfacial capillary forces¹⁷ to drive the QDs into lithographically patterned holes in the bowtie gaps. This simple method avoids additional steps such as chemical modification of the QD/nanostructure surfaces. The process, described in Figure 1 and in the Methods section, led to the trapping in bowtie gaps of a number of QDs that varied from one to several, as could be ascertained by scanning electron microscopy.

Dark field microspectroscopy was used in order to characterize the plasmonic behavior of every single bowtie by measuring its scattering spectrum. As shown in Supplementary Figure 1, empty bowties possess two modes, a transverse mode at ≈ 2.05 eV and a longitudinal mode at ≈ 1.9 eV, the latter being due to dipolar coupling of the two parts of each bowtie. The absorption and emission spectra of the QDs are shown in Supplementary Figure 2, and demonstrate that the optical transitions of the QDs are in resonance with the plasmon excitations of the bowties.

Figure 2a shows bowties with QDs in their gaps whose scattering spectra present transparency dips indicative of Rabi splitting. Overall we collected scattering spectra from 21 QD bowties, out of which 14 spectra showed a definite signature of splitting. Thus, the top bowtie in Figure 2a, with a single QD and a particularly small gap (~ 18 nm), presents a clear Rabi splitting feature. Similarly, Rabi splitting is observed in the spectra of the two other bowties shown in Figure 2a, with two and three QDs, respectively. The spectra in this figure, as well as other spectra showing Rabi splitting, were fitted using the coupled oscillator model¹⁸ (see Methods). This model represents the plasmon mode and the exciton of the quantum emitter as coupled harmonic oscillators exchanging energy reversibly. The coupling

leads to the generation of upper (Ω_+) and lower (Ω_-) plasmon-exciton hybrid states, with a transparency dip in between^{13,19}. The latter appears when the coupling rate, g , and the linewidths of the plasmon and emitters spectra (γ_{pl}, γ_0) are of the same order of magnitude, and are also approximately related in the following manner: $g^2 > (\gamma_{pl} - \gamma_0)^2/16$. The Rabi splitting values, $\Omega_+ - \Omega_-$, can be obtained directly from the fitted curves, and for the three examples in Figure 2a they are 176, 288 and 224 meV, respectively. These values are comparable to recently reported values of coupling rates of J-aggregates with individual plasmonic structures^{6,7}, where hundreds of quantum emitters were involved. Not all bowties loaded with a single QD showed a clear transparency dip in the scattering spectrum. Instead, Rabi splitting manifested itself in a significant spectral broadening as compared to that of an empty bowtie (Supplementary Figure 3), indicating coupling between plasmons and excitons. Splitting was readily observed in bowties with several QDs- see Supplementary Figure 4 for additional spectra.

A plot of Rabi splitting values vs. gap size for data sets with 1-3 QDs is shown in Figure 2b, which demonstrates that, as expected, the coupling increases with the number of quantum emitters (N) ($g \approx \sqrt{N}g_1$, g_1 being the coupling rate for one quantum emitter¹). The Rabi splitting also depends on the gap size of each bowtie. For instance, for two QDs the Rabi splitting is more than doubled when the gap size changes from 25 to 17 nm. Though the values of the coupling rates obtained from the fits are smaller than the values of the plasmon widths (which are ~ 400 meV), significant splittings are observed, indicating that the strong coupling regime has indeed been attained¹¹. Supplementary Figure 5 shows histograms of the values of all parameters obtained from the coupled oscillator fits to measured spectra.

To obtain an unequivocal proof that the splitting in the spectra is due to strong (or close-to-strong) coupling of the bowtie longitudinal plasmon mode and the quantum emitter's

exciton, we resorted to polarization-dependent experiments, in which the polarization of the excitation source was rotated. Figure 2c shows an example of a polarization series measured on the bowtie with two QDs from Figure 2a. When the excitation is polarized along the longitudinal direction of the bowtie (i.e. along its long axis) the spectrum shows two peaks due to Rabi splitting. As the polarization is rotated to the transverse direction the double-peaked spectrum is gradually replaced with the single-peaked spectrum of the transverse mode. Similar results with other bowties are shown in Supplementary Figure 6. These results clearly indicate that the transparency dips in the scattering spectra are due to a bona fide coupling of the plasmon and QD excitations.

Electromagnetic calculations were carried out to support the experimental results, using the boundary element method²⁰. The simulations revealed some interesting facts. Figure 3a shows the calculated scattering spectrum of an empty bowtie at the top. The spectrum for a bowtie with a single QD at the center of the gap is shown below, demonstrating a small change compared to the empty bowtie. However, when the QD is positioned closer to one of the triangles constituting the bowtie, or the number of QDs in the hotspot is increased from one to two, a more significant transparency dip appears. Importantly, *no such splitting is found* when the simulation is repeated with a single metallic prism rather than a bowtie structure.

The simulation allows us to directly calculate the coupling rate for a quantum emitter with an oscillator strength similar to a QD (~ 0.6). The spatial distribution of the coupling rate across the gap is shown in Figure 3b, clearly indicating that the electromagnetic field in the hot spot is not uniform and is concentrated at the edges rather than at the center. Indeed, in many of the bowties exhibiting strong coupling (Figure 2 and Supplementary Figures 3 and 4) the QDs are close to one of the edges, in agreement with the simulation results. We

estimate from the simulation that at the center of a bowtie structure g is ~ 100 meV, while very close to one of the triangles g is as high as 200 meV.

In conclusion, we have successfully integrated lithographically fabricated silver bowties with one to a few QDs that reside exactly within the plasmonic cavity. The very small plasmon mode volumes of the bowties allowed us to demonstrate vacuum Rabi splitting in the limit of an individual quantum emitter. Rabi splitting as high as ~ 180 meV was observed with a single QD. This achievement paves the way to novel quantum optics and quantum information experiments within plasmonic systems and at room temperature. Future work will further increase the coupling by reducing the mode volume of the bowties, which can be achieved by decreasing their gap size and improving control on their shape, and by further improvement in QD positioning methodology.

Methods

Materials. Glass/ITO (10 mm \times 10 mm \times 1.1 mm) substrates were purchased from Xin Yan Technology Ltd., China. The ITO layer is 180 nm thick, and is characterized by 83 % transparency to visible light and a sheet resistance of 10 ohm/sq. Poly(methyl methacrylate) 950K A2 (PMMA) electron beam resist, used for the fabrication of bowties, was procured from MicroChem. Chromium (used as an adhesive layer) and silver were obtained from Kurt J. Lesker. Water soluble, mercapto-undecanoic acid capped CdSe/ZnS core/shell nanocrystals (quantum dots) were acquired from MK Impex Corp.

Electron Beam Lithography and Fabrication of Silver Bowties. Prior to fabrication, Glass/ITO substrates were cleaned with acetone followed by isopropanol for 3 minutes in each step. The cleaned glasses were dried using a nitrogen flow and then PMMA was spin-

coated at a speed of 6000 rpm for 50 sec to achieve a thickness of 60 nm, followed by baking at 180°C for 90 sec. The PMMA-coated glasses were loaded into a Raith E_line Plus electron beam lithography system and the PMMA was exposed to define the shape of bowties. The accelerating voltage used for the exposure was 30 kV and the beam current was 30 pA. The design consisted of matrices of bowties, with each matrix hosting 64 bowties. Each bowtie was separated by 10 μm from its neighboring partner to guarantee no interaction. To remove the exposed PMMA, the substrates were developed using 1:3 methyl isobutyl ketone:isopropyl alcohol for 30 sec, followed by immersion in a stopper (isopropyl alcohol) for 30 seconds and drying with a nitrogen flow.

An electron beam evaporator (Odem) was used for the metal deposition on the patterned substrates. Initially chromium was evaporated to deposit a 2 nm adhesion layer, followed by silver. Different prism lengths from 75 to 200 nm and thicknesses from 20 to 35 nm were examined and finally the dimensions were fixed to a length of ≈ 85 nm and a thickness of ≈ 30 nm. These bowties showed a plasmon resonance that overlapped the QD exciton frequency. After metallization a liftoff step was performed in acetone for 5 minutes to obtain silver bowties on the glass/ITO substrate.

A second stage of E-beam lithography was performed in order to expose holes in the gap regions of the bowties. A 60 nm layer of PMMA was spin coated on the substrate and then the gap regions of the bowties were exposed to create 10-30 nm holes, into which the QDs were driven. (See below and in Figure 1 of the main text.) This exposure was facilitated by using alignment marks that were fabricated in the first E-beam exposure step, and which enabled reaching an overlay accuracy as high as a few nanometers.

Incorporation of QDs into bowtie structures. To incorporate QDs into the bowtie gaps we adopted a method originally developed by Alivisatos and coworkers¹⁷. Substrates with

bowties and holes in the PMMA layer prepared as described above were placed vertically in an aqueous solution of QDs. Controlled solvent evaporation was then used to exert a capillary force along the receding line of contact of the QD solution and drive QDs successfully into the holes. By varying the QD concentration in solution (from 10 to 100 nM), bowties with one to a few QDs in the gap were successfully obtained (Figure 1). Though this method is limited in controlling the exact position of the QDs within the gap, it was found to be facile and relatively reproducible.

Bulk Absorption and Emission Measurements of QDs. Steady state absorption and emission spectral measurements (Supplementary Figure 2) were carried out on a Cary-100 UV-VIS spectrophotometer (Varian) and a Fluorolog-3 spectrofluorimeter (Horiba Jobin Yvon), respectively. Extinction coefficients of the QDs were estimated by employing the method developed by Peng and coworkers²¹.

Dark-field Microspectroscopy. Scattering spectra of every single bowtie with and without QDs were measured with an inverted microscope equipped with a dark field condenser, a 75 W Xenon lamp (Olympus) and a 100× oil immersion objective with NA = 1.30. A SpectraPro-150 spectrograph with a 1200 g/mm grating (Acton) and a Newton spectroscopy CCD camera (Andor Technology) were used to disperse scattered photons and register spectra. Raw spectra were smoothed using a Fourier low-pass filter. Prior to the spectral measurements the camera was calibrated in reference to the spectrum of fluorescent dyes. Polarization of the excitation light was controlled by a combination of a polarizer and a selecting sector, such that essentially only s-polarized light reached the sample.

Data fitting to the coupled-oscillator model. Scattering spectra were fitted to the following equation, which represents the scattering of two coupled harmonic oscillators at frequency ω

$$\sigma_{sca}(\omega) = A\omega^4 \left| \frac{(\omega^2 - \omega_0^2 + i\omega\gamma_0)}{(\omega^2 - \omega_0^2 + i\omega\gamma_0)(\omega^2 - \omega_{pl}^2 + i\omega\gamma_{pl}) - \omega^2 g^2} \right|^2 \dots \dots \dots (1)$$

In this expression ω_{pl} and ω_0 are the plasmon and QD resonance frequencies, respectively, while γ_{pl} and γ_0 are the corresponding linewidths. g is the coupling rate and A is a scaling parameter. Parameters obtained from fits to all our data sets are shown in Supplementary Figure 5. We fixed the value of γ_0 to 130 meV, which is the measured linewidth of the fluorescence spectra of individual QDs (not shown). In the case of some of the data sets with a single QD in the gap, where broadening of the spectrum was observed, though no clear splitting, we also fixed the value of γ_{pl} to 385 meV, which is the average value of this parameter obtained from multiple spectra of empty bowties.

Electromagnetic Simulations. Numerical simulations of the silver bowties were performed using the boundary-element method as implemented in MNPBEM – a toolbox developed by Hohenester and co-workers.²⁰ A numerical model of a bowtie was constructed from two prisms with equilateral triangular bases of 80 nm side length, 30 nm heights, radii of curvature at the vertices of 7 nm, and a gap size of 17 nm. The complex refractive index of silver from Johnson and Christy²² was used, and a refractive index of 1.33 was assumed for the ambient medium. The bowtie was excited by a plane wave at normal incidence and polarized along the longitudinal direction and the plasmon scattering spectra were calculated at the far field. From the spectrum of an unloaded cavity we calculated $\gamma_{pl}=0.25$ eV, which is smaller than the typical experimental linewidth. However, the cavity quality factor: $Q = \omega_{pl}/\gamma_{pl}=7.3$, was only slightly higher than the measured quality factor. Simulations of scattering spectra for a bowtie loaded with QDs were performed with dots modeled as spheres of 8 nm located at various positions within the gap. The complex dielectric function of these dots was approximated by a Lorentz model with a high-frequency dielectric constant

$\epsilon_\infty=6.1$, $\omega_0=1.8$ eV, $\gamma_0=0.08$ eV, and an oscillator strength $f=0.6$ ^{21,23,24} Note that the QD linewidth used was scaled to match the computed plasmon linewidth, which is smaller than the measured one.

The position-dependent coupling rate of a QD strongly coupled to the bowtie $g(r) = \mu \cdot E(r)/\hbar$, with μ being the transition dipole moment of the QD and \hbar the reduced Planck constant, was evaluated using $E(r)$, the electric field numerically calculated at the plasmon resonance energy $\omega_{pl}=1.83$ eV. To this end, the mode volume of the antenna was calculated using the approach of Koenderink²⁵, and was used to normalize the energy density within the cavity, assuming it is occupied with a single photon of energy 1.83 eV. A map of $\hbar g(r)$ plotted on a horizontal plane that intersects the bowtie at its half-height is shown in Figure 3b.

References

- 1 Haroche, S. & Raimond, J. M. *Exploring the Quantum: Atoms, Cavities and Photons*. 1 edn, (Oxford University Press, 2006).
- 2 Hennessy, K. *et al.* Quantum nature of a strongly coupled single quantum dot-cavity system. *Nature* **445**, 896-899 (2007).
- 3 Monroe, C. Quantum information processing with atoms and photons. *Nature* **416**, 238-246 (2002).
- 4 Lo, H. K. & Chau, H. F. Unconditional security of quantum key distribution over arbitrarily long distances. *Science* **283**, 2050-2056 (1999).
- 5 Kimble, H. J. The quantum internet. *Nature* **453**, 1023-1030 (2008).
- 6 Schlather, A. E., Large, N., Urban, A. S., Nordlander, P. & Halas, N. J. Near-field mediated plexcitonic coupling and giant Rabi splitting in individual metallic dimers. *Nano Lett* **13**, 3281-3286 (2013).
- 7 Zengin, G. *et al.* Realizing Strong Light-Matter Interactions between Single-Nanoparticle Plasmons and Molecular Excitons at Ambient Conditions. *Phys Rev Lett* **114**, 157401 (2015).
- 8 Yoshie, T. *et al.* Vacuum Rabi splitting with a single quantum dot in a photonic crystal nanocavity. *Nature* **432**, 200-203 (2004).
- 9 Reithmaier, J. P. *et al.* Strong coupling in a single quantum dot-semiconductor microcavity system. *Nature* **432**, 197-200 (2004).
- 10 Brongersma, M. L. & Shalaev, V. M. Applied physics. The case for plasmonics. *Science* **328**, 440-441 (2010).
- 11 Torma, P. & Barnes, W. L. Strong coupling between surface plasmon polaritons and emitters: a review. *Rep Prog Phys* **78**, 34 (2015).
- 12 Zengin, G. *et al.* Approaching the strong coupling limit in single plasmonic nanorods interacting with J-aggregates. *Sci Rep* **3**, 3074 (2013).
- 13 Savasta, S. *et al.* Nanopolaritons: vacuum Rabi splitting with a single quantum dot in the center of a dimer nanoantenna. *ACS Nano* **4**, 6369-6376 (2010).
- 14 Schuck, P. J., Fromm, D. P., Sundaramurthy, A., Kino, G. S. & Moerner, W. E. Improving the mismatch between light and nanoscale objects with gold bowtie nanoantennas. *Phys Rev Lett* **94**, 017402 (2005).
- 15 Ru, E. C. L. & Etchegoin, P. G. *Principles of Surface Enhanced Raman Spectroscopy*. (Elsevier, 2009).
- 16 Leistikow, M. D., Johansen, J., Kettelarij, A. J., Lodahl, P. & Vos, W. L. Size-dependent oscillator strength and quantum efficiency of CdSe quantum dots controlled via the local density of states. *Phys Rev B* **79**, 045301 (2009).
- 17 Cui, Y. *et al.* Integration of colloidal nanocrystals into lithographically patterned devices. *Nano Lett* **4**, 1093-1098 (2004).
- 18 Wu, X., Gray, S. K. & Pelton, M. Quantum-dot-induced transparency in a nanoscale plasmonic resonator. *Opt Express* **18**, 23633-23645 (2010).
- 19 Rudin, S. & Reinecke, T. L. Oscillator model for vacuum Rabi splitting in microcavities. *Phys Rev B* **59**, 10227-10233 (1999).
- 20 Hohenester, U. & Trügler, A. MNPBEM – A Matlab toolbox for the simulation of plasmonic nanoparticles. *Comp Phys Comm* **183**, 370-381 (2012).
- 21 Yu, W. W., Qu, L., Guo, W. & Peng, X. Experimental determination of the extinction coefficient of CdTe, CdSe, and CdS nanocrystals. *Chem Mater* **15**, 2854-2860 (2003).
- 22 Johnson, P. B. & Christy, R. W. Optical Constants of the Noble Metals. *Phys Rev B* **6**, 4370-4379 (1972).
- 23 Alivisatos, A. P., Harris, T. D., Carroll, P. J., Steigerwald, M. L. & Brus, L. E. Electron-vibration coupling in semiconductor clusters studied by resonance Raman-spectroscopy. *J Chem Phys* **90**, 3463-3468 (1989).

- 24 Leistikow, M. D., Johansen, J., Kettelarij, A. J., Lodahl, P. & Vos, W. L. Size-dependent oscillator strength and quantum efficiency of CdSe quantum dots controlled via the local density of states. *Phys Rev B* **79**, 9 (2009).
- 25 Koenderink, A. F. On the use of Purcell factors for plasmon antennas. *Opt Lett* **35**, 4208-4210 (2010).

Acknowledgements

GH is the incumbent of the Hilda Pomeraniec professorial chair. We thank Dr. Barak Dayan for useful comments on the manuscript.

Author Contributions

SK, OB and GH designed the research. SK and OB performed the experiments. LC performed electromagnetic simulations. All authors participated in writing the manuscript.

Competing financial interests

The authors declare no competing financial interests.

Figure legends

Figure 1. Construction of bowties with quantum dots in their gaps. **a**, Schematic illustration of the two-step lithography process for making holes at the center of bowtie structures and the interfacial capillary force assisted method for driving QDs into the holes. **b**, Scanning electron microscope images of bowties with one, two and multiple QDs in their gaps (from top to bottom). The positions of the QDs are marked by red arrows. Yellow scale bars represent 20 nm.

Figure 2. Strong coupling of plasmons and quantum emitters. **a**, Scattering spectra of bowties with (from top to bottom) one, two and three QDs in the gap, respectively. All spectra show a transparency dip due to Rabi splitting. The black lines are experimental data, and the colored lines are fits to the coupled oscillator model. Insets show the scanning electron microscope images of the bowties. The positions of the QDs are marked by red arrows. Yellow scale bars represent 20 nm. **b**, Rabi splitting as a function of gap size for bowties with one, two and three QDs (yellow, green and blue symbols, respectively). The errors in the Rabi splitting values, obtained from the fitted functions, are estimated to be $\sim 10\%$. **c**, Polarization series of the middle bowtie structure in **a**. As the polarization of the excitation light is rotated from the direction parallel to the bowtie long axis to perpendicular to it, the transparency dip in the spectrum gradually vanishes, indicating that it indeed originates in the strong coupling of the QD exciton with the longitudinal plasmon resonance of the bowtie.

Figure 3. Electromagnetic simulations of strongly-coupled plasmonic structures. **a**, Simulated scattering spectra of bowties with one and two QDs organized as indicated in the inset structures. **b**, Distribution of the coupling rate (in eV) of a quantum emitter with an oscillator strength of 0.6 in a bowtie structure.

Figures

Figure 1

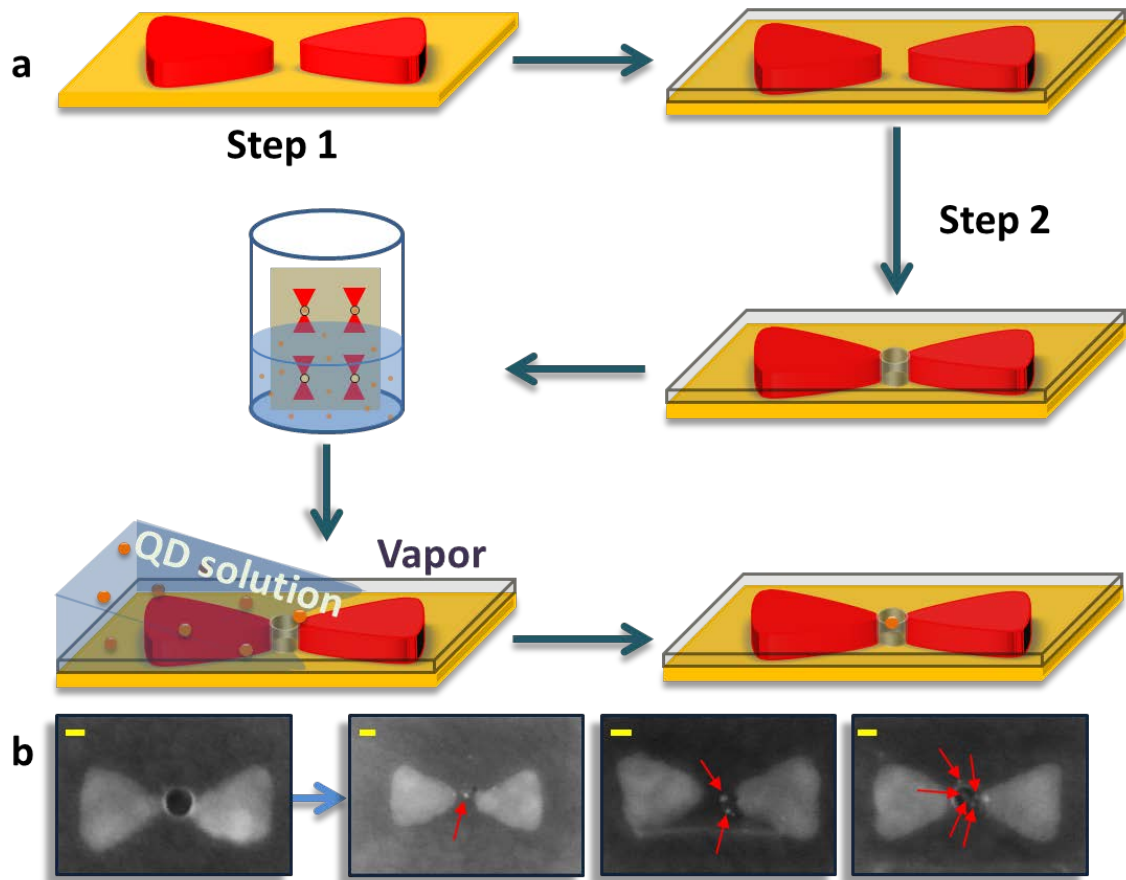


Figure 2

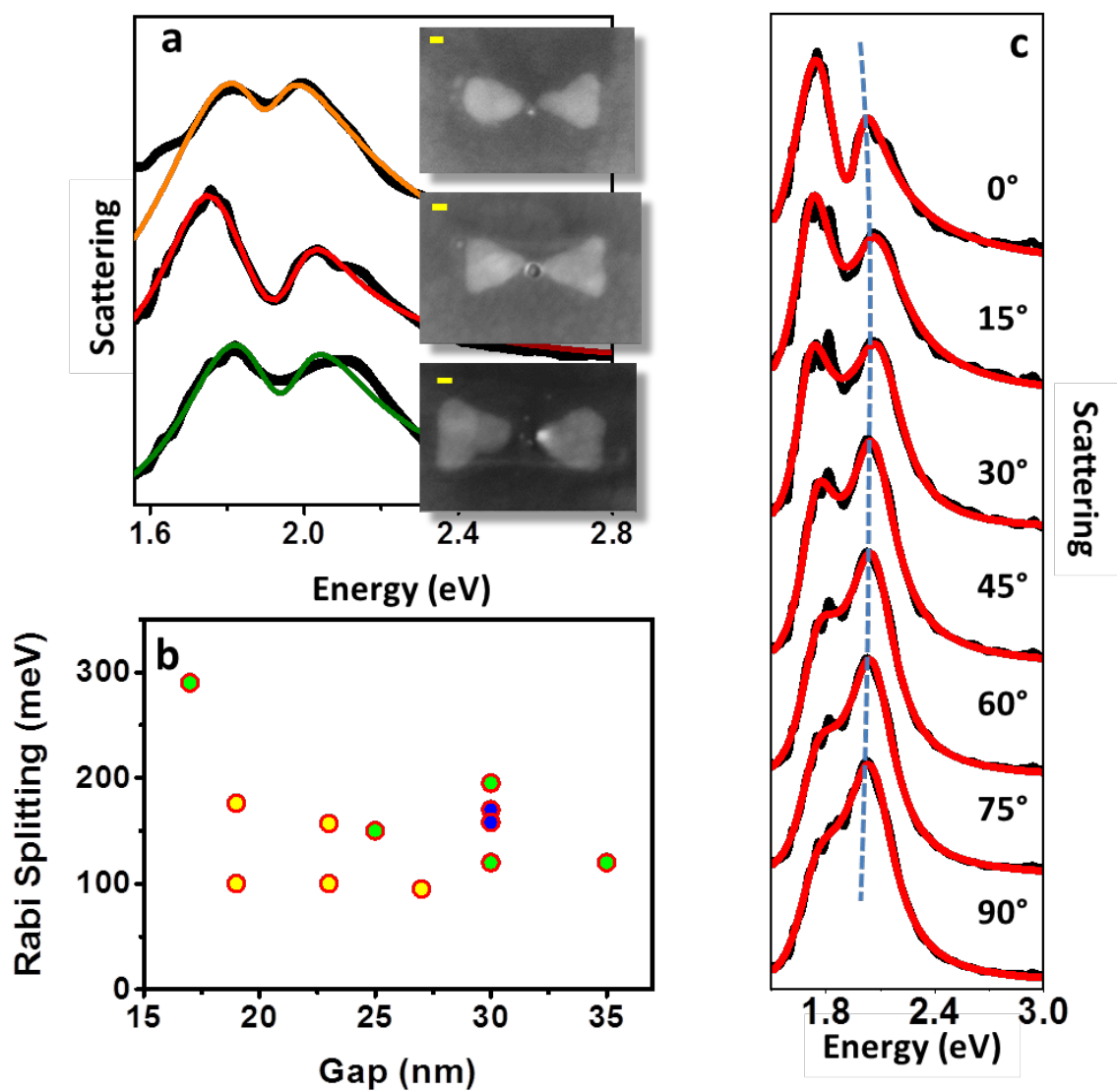
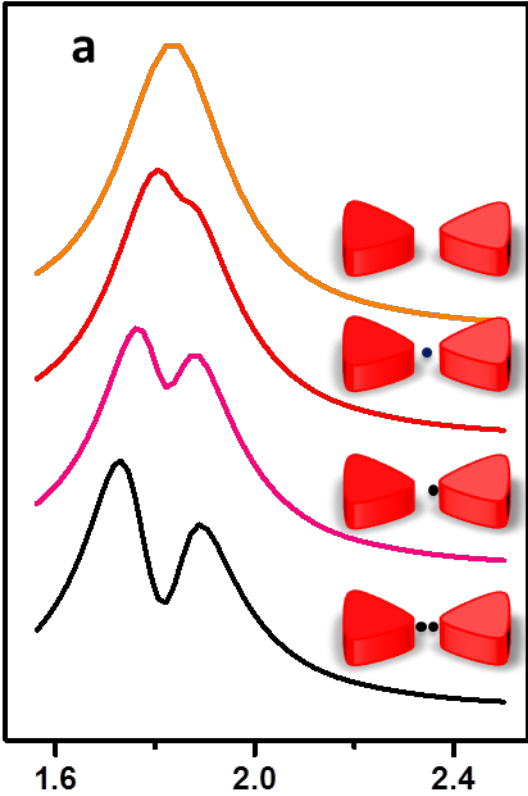
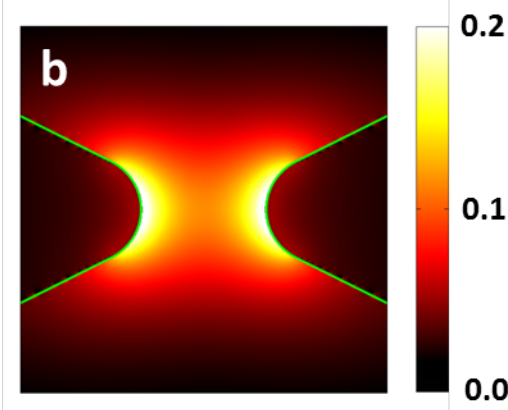


Figure 3



Energy (eV)

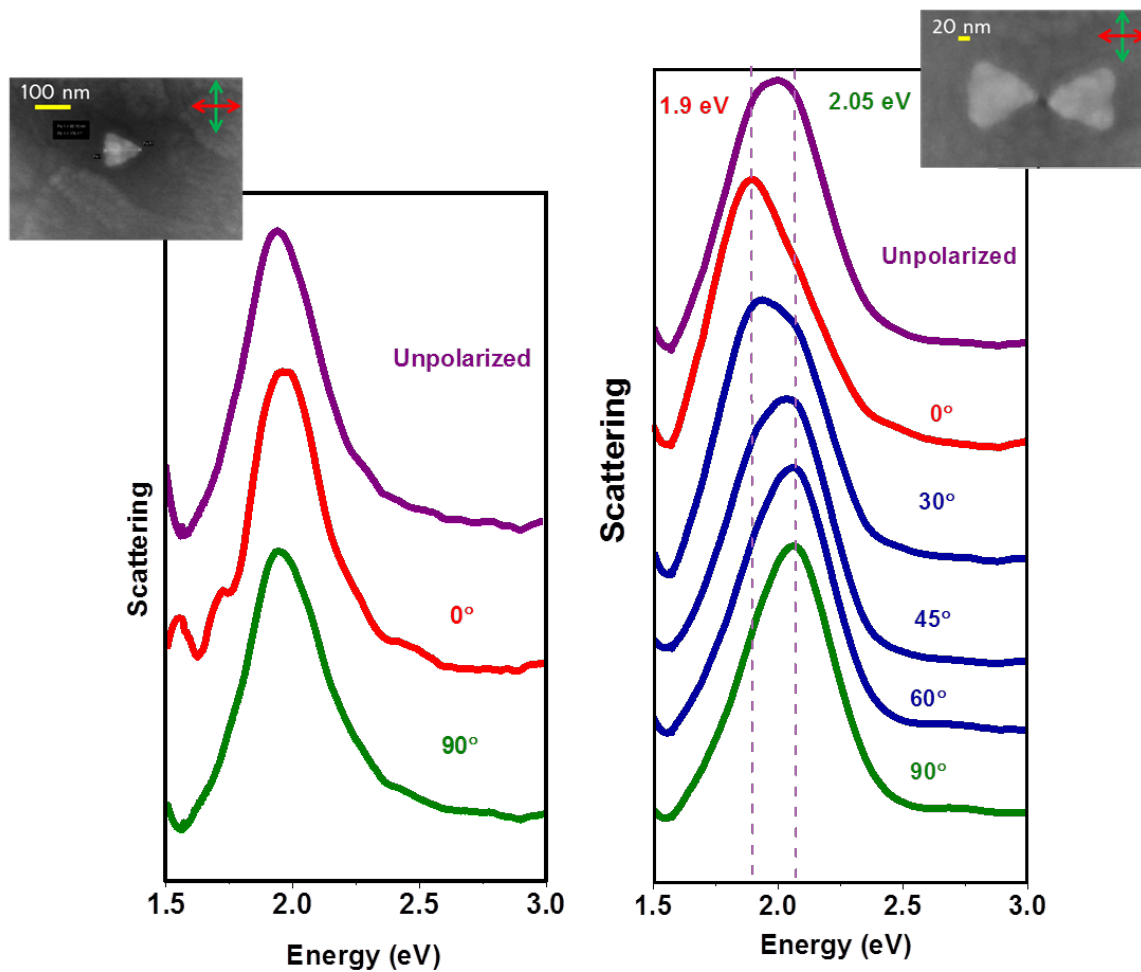


Supplementary Information

Vacuum Rabi splitting in a plasmonic cavity at the single quantum emitter limit

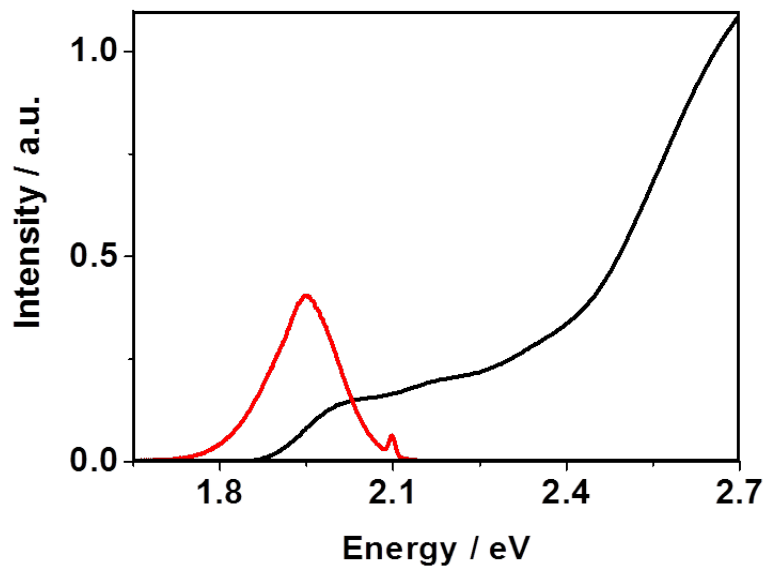
Kotni Santhosh^{1,*}, Ora Bitton^{2,*}, Lev Chuntonov^{3,*} and Gilad Haran¹

Supplementary Figure 1



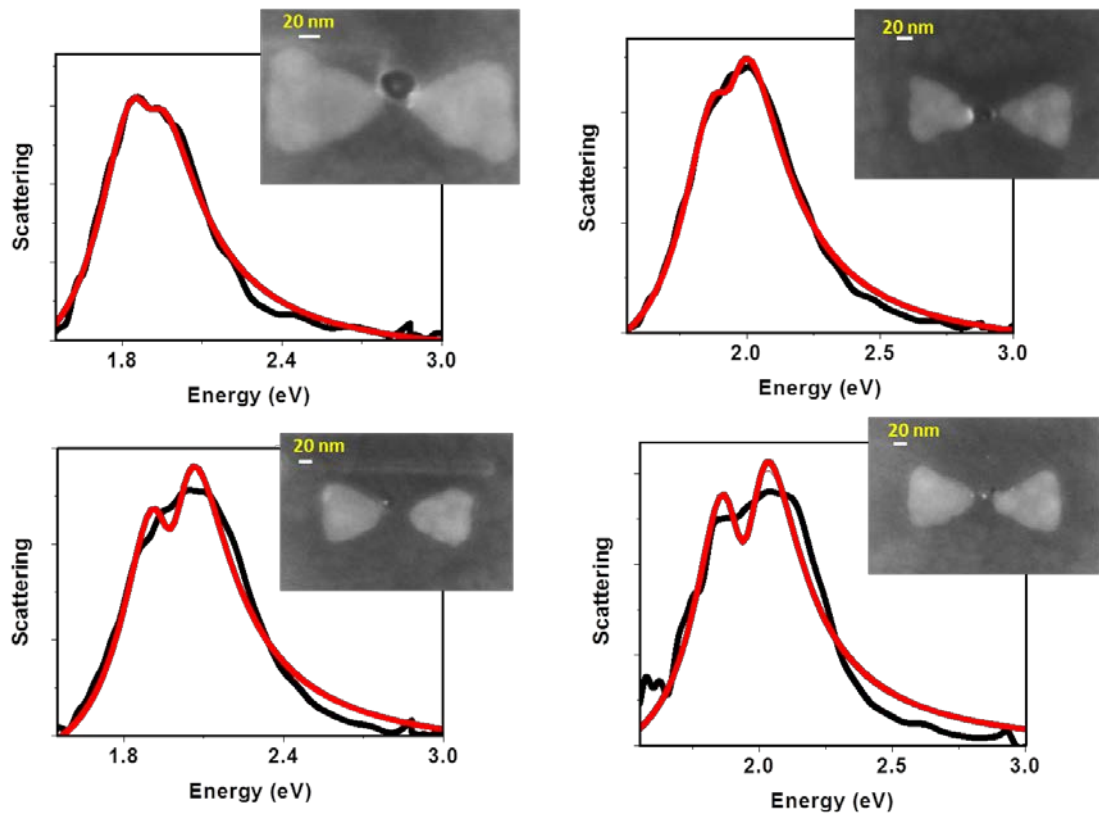
Dark field scattering spectra of an individual prism and an individual bowtie as a function of angle of polarization. The corresponding electron microscope images of the structures are also shown. Red and green arrows denote the direction of polarization parallel to the bowtie axis and perpendicular to it, respectively. The solid lines are smoothed versions of the data.

Supplementary Figure 2



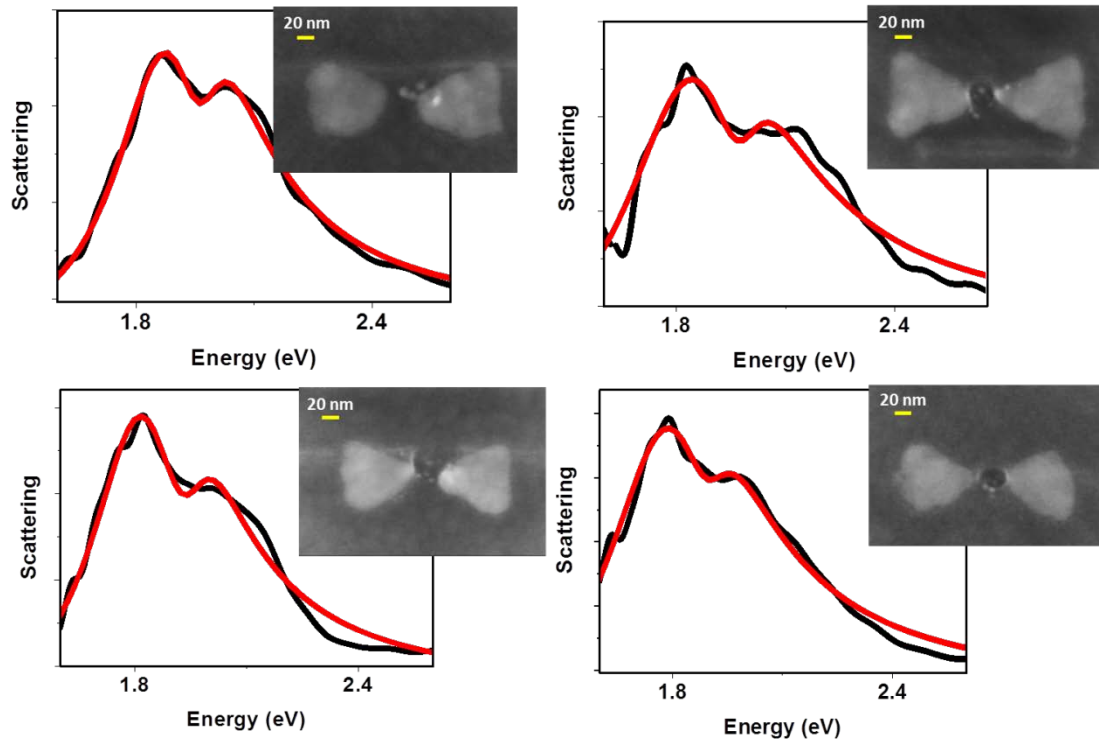
Spectroscopy of quantum dots in water. The figure shows absorption (black) and emission (red) spectra of CdSe/ZnS QDs in water. The lowest energy optical transition of the QDs (at 1.9 eV \approx 660 nm) is at resonance with the longitudinal plasmon excitation seen in Supplementary Figure 1.

Supplementary Figure 3



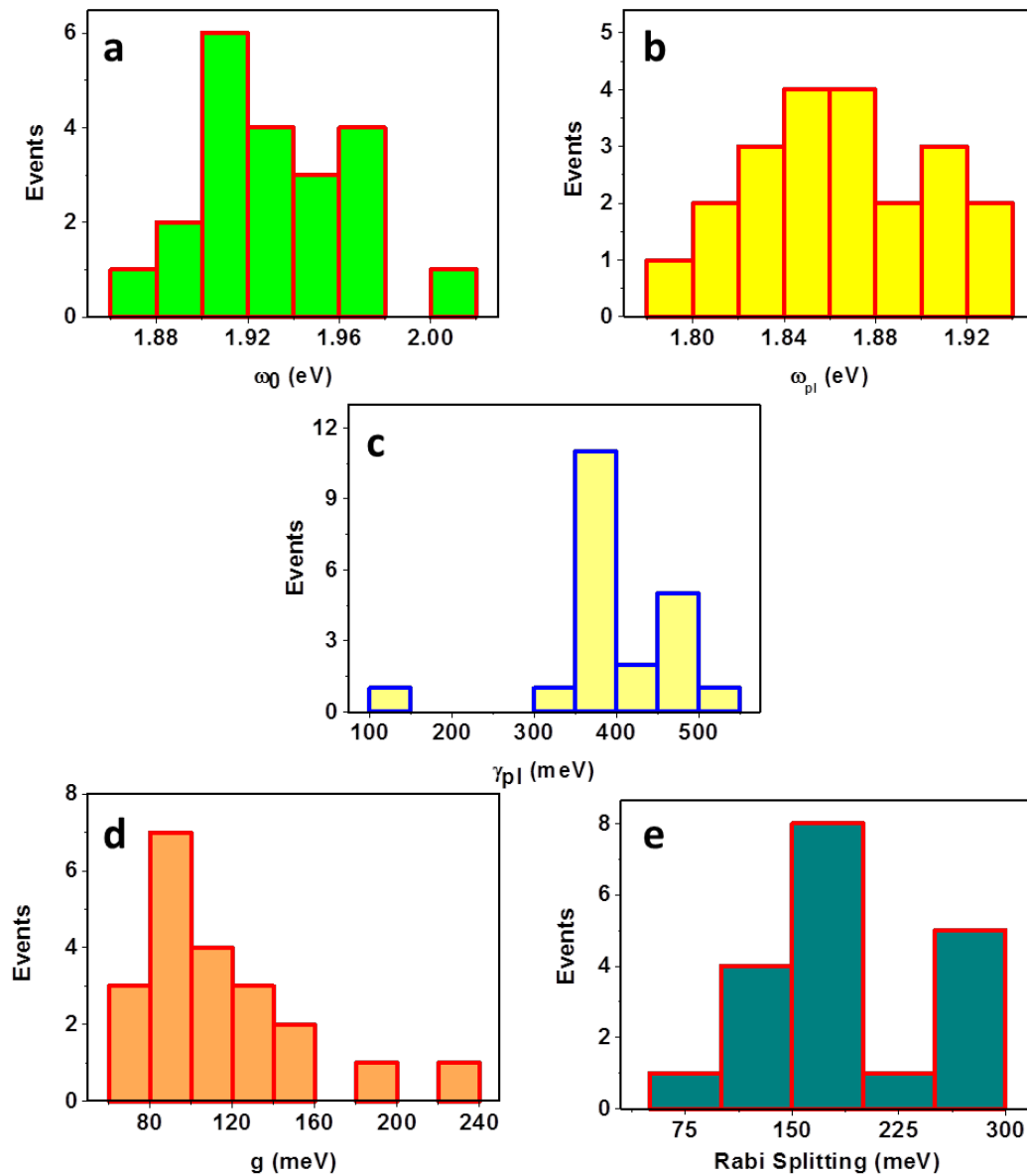
Scattering spectra and corresponding electron microscope images of bowties with a single QD in their gaps. Red solid lines are fits to the coupled oscillator model. For these fits we fixed the value of the plasmon linewidth to the average value measured from empty bowties, 0.385 eV. The coupled oscillator model does not fit the two bottom spectra well, but the structure of the spectra and their widths clearly point to splitting (compare with Supplementary Figure 1).

Supplementary Figure 4



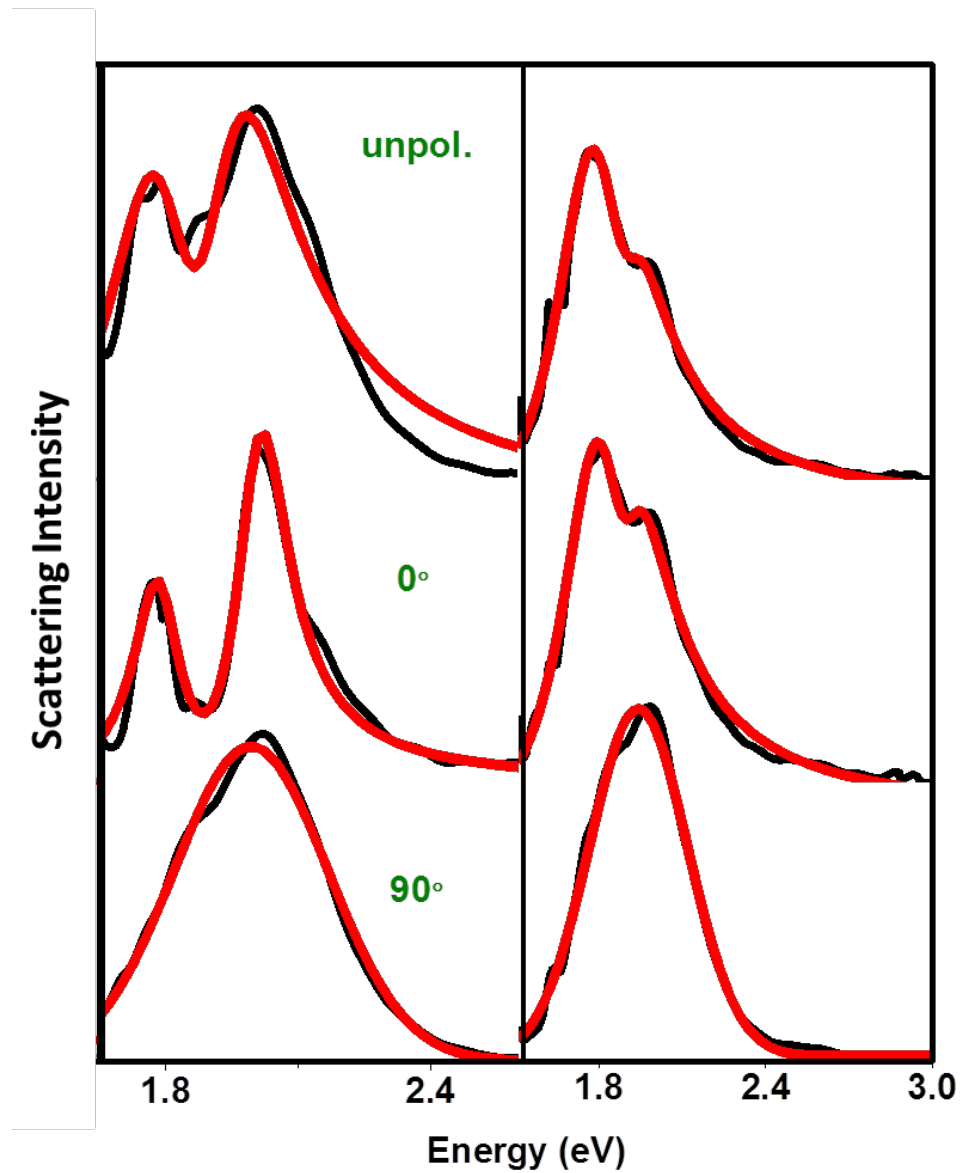
Scattering spectra of bowties with several QDs within the gap. The insets show scanning electron microscope images of the bowties. The red solid lines are fits to the coupled oscillator model.

Supplementary Figure 5



Parameters from coupled oscillator model fits to scattering spectra. The figure shows the fitting parameters obtained from fits of scattering spectra to the coupled oscillator model (equation 1 in Online Methods). a. Resonance frequency of the quantum emitter(s). b. Plasmon resonance frequencies. c. Plasmon linewidths. d. Coupling rates. e. Rabi splittings calculated directly from the fitted spectra.

Supplementary Figure 6



Polarization dependence of scattering spectra. Rabi splitting is observed when the laser polarization is parallel to the bowtie long axis (0°), but it vanishes when the polarization is rotated by 90° .